JOURNAL OF Applied Polymer SCIENCE

# Natural Rubber Protein as Interfacial Enhancement for Bio-Based Nano-Fillers

**Lei Jong**
Department of Agriculture, National Center for Agricultural Utilization Research, 1815 N. University St., Peoria, Illinois 61604
Correspondence to: L. Jong (E-mail: lei.jong@ars.usda.gov)

**ABSTRACT:** Natural rubber was enhanced with soy protein nano-aggregates and carbon black using a hybrid process. The rubber composites reinforced with an optimum amount of soy protein or soy protein/carbon black showed useful tensile properties. The stress-strain behaviors were analyzed with a micro-mechanical model that describes the stress–strain measurements well. The model analysis provides insight into filler network characteristics and entanglement modulus. The composites were also analyzed with both linear and nonlinear viscoelastic properties. Temperature and frequency dependent modulus as well as the model analysis of stress softening effect describe the ability of soy protein to constraint polymer chains in the highly filled composites. For the composites reinforced with soy protein, the good tensile properties are attributed to good filler-polymer adhesion through the compatibilization effect of natural rubber protein. © 2013 Wiley Periodicals, Inc. J. Appl. Polym. Sci. 000: 000–000, 2013

**KEYWORDS:** rubber; mechanical properties; biomaterial; viscoelasticity

Received 16 December 2012; accepted 11 March 2013; Published online
**DOI: 10.1002/app.39277**

## INTRODUCTION

Natural rubber is a major rubber raw material in addition to styrene-butadiene rubber. Natural rubber latex is a natural polymer of isoprene, mostly cis-1,4-polyisoprene[1,2] and its stereoregularity contributes to the strain-induced crystallization as well as good green and tensile strength. Typically, a small percentage (up to 5% of dry mass) of other materials, such as proteins, fatty acids, carbohydrates, phospholipids and inorganic salts, are found in natural rubber.[2,3] The role of these nonrubber cmponents and their interactions with polyisoprene have been studied.[4–6] Natural rubber has applications in seals, automobile belts, hoses, tire treads, and various types of molded objects. Mechanical properties of natural rubber are often adjusted with different types of fillers that have different particle size and surface energy for different applications. Conventional fillers include both carbonized organic compounds and inorganic particles. The major fillers represent these two categories are carbon black and silica of various aggregate size and surface treatments. Carbon black dominates about 90% of the rubber filler market. Carbon black is produced by the combustion of petroleum oil or natural gas with a yield less than 50% and generates carbon dioxide as the main by-product. Recently, some natural materials such as cellulose[7,8] and starch[9,10] have been under development to improve mechanical properties of rubbers. Natural materials have advantages of being renewable, sustainable, light weight, carbon neutral, and biodegradable. However, more knowledge is required to develop useful applications from a variety of renewable materials, especially on how the natural materials interact with other materials in different material constructions. The mechanical properties of rubber composites depend on the filler and polymer structures, as well as processing methods. When the same filler and rubber are used, the composite properties depend on the processing methods because processing methods yield different filler network structure. Rubber composites prepared by blending carbon black and rubber latex gave rise to different mechanical properties than those prepared with traditional melt-processing method.[11] For bio-fillers, rubber composites prepared with casting method usually have higher elastic modulus; those prepared with melt-process have a lower elastic modulus because of different structure formation. Renewable fillers can be incorporated in different ways, either by direct melt blending or mixed with rubber latex. It is well known that filler size and filler surface properties are important factors to improve the strength of rubber.[12]

Mention of trade names or commercial products in this publication is solely for the purpose of providing specific information and does not imply recommendation or endorsement by the U.S. Department of Agriculture. USDA is an equal opportunity provider and employer.

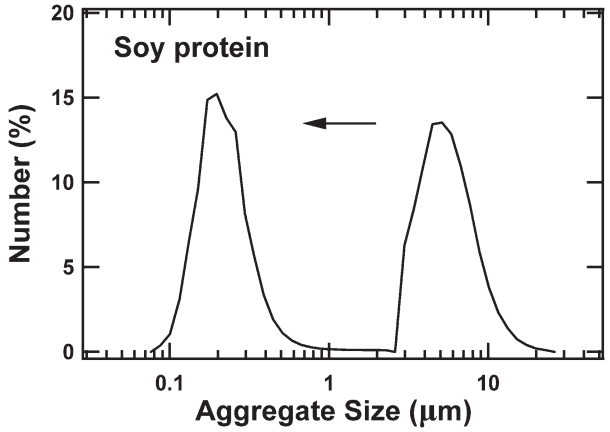


**Figure 1.** Soy protein nano-aggregates produced from microfluidizer after processed for 12 cycles at pH 9. The mean size changed from 5.6 $\mu$m to 150 nm.

Generally, smaller filler size and strong interactions between filler and rubber matrix tend to improve the rubber modulus.[13] Soy protein extracted from soybean is a renewable, reliable and abundant sustainable material source. Although soy protein has been largely used in food applications, soy protein is a fractal-like nanoparticle aggregate[14–16] formed from ~10 nm protein units and is rigid with an elastic modulus of 2 GPa,[17] which makes soy protein an interesting biomaterial to enhance mechanical properties of soft polymers. Soy protein, a polypeptide, has a polyamide structure formed from the condensation reaction between amino acids. In this study, the size of soy protein particles was economically reduced by using a microfluidizer and then blended with natural rubber latex. The dried rubber/soy protein mixture was then melt-processed with carbon black and other rubber chemicals using traditional rubber compounding process. These new composites were characterized with stress–strain, linear and nonlinear viscoelastic properties, which were analyzed with models to provide greater insight into the filler network structures.

## EXPERIMENTAL

### Materials

The soy protein isolate (SP) (Ardex F) used in this research was a spray dried powder (Archer Daniels Midland Company, Decatur, IL). The SP contained ~90% soy protein, ~5% ash, and ~5% fat. Sodium hydroxide, used to adjust pH, was ACS grade. The natural rubber (NR) latex used was Centex LATZ obtained from Centrotrade Rubber (Chesapeake, VA). The glass transition temperature, determined by $G''$ maximum, of a crosslinked NR with 2 phr (parts per hundred parts of rubber) sulfur was $-60°C$. The NR latex received had ~61% solids and a pH ~10. Carbon black used in this study is N-339 (Vulcan M from Cabot Corporation, Alpharetta, GA), which is an aggregate[18] consisted of ~39 nm primary particles. The aggregates have a weight mean diameter of ~122 nm and a surface area of ~96 $m^2$/gm. Other rubber compounding ingredients including antioxidant (2,2′-Methylenebis(6-tert-butyl-4-methylphenol)), sulfur, stearic acid, and zinc oxide were purchased from Sigma-Aldrich (St. Louis, MO). Accelerator, N-cyclohexyl-2-benzothiazolesulfenamide (CBTS), was purchased from Akrochem (Akron, OH).

### Preparation of Natural Rubber Blends with Soy Protein Nano-Aggregates

Soy protein were first wetted in distilled water by homogenizing it at $10^4$ rpm for 10 min, and followed by adjusting the pH of the dispersion to 9 with dilute sodium hydroxide. The dispersion was further homogenized for 20 min before it was fed to a microfluidizer (M-100P, Microfluidics, Newton, MA) equipped with a diamond interaction chamber (200 $\mu$m), and operated at a pressure of 159 MPa. The dispersions were passed through the microfluidizer continuously and the samples were collected after 12 cycles. The temperature of the dispersion was controlled by a continuous stream of cold water flowing through a water container, where an outlet coil was immersed. The particle distribution of the resulted soy protein nano-aggregates is shown in Figure 1.The soy protein dispersion was blended with natural rubber latex at pH 9 and dried under ambient condition until the moisture content is less than 5%. Four blends containing different amount of soy protein were prepared so that the final formulations in rubber compounding have a soy protein to carbon black ratio of 1/3, 1/1, and 3/1.

### Particle Sizing

The mean particle size and distribution of protein aggregates were measured using a Horiba LA-930 laser scattering particle size analyzer (Horiba Instruments, Irvine, CA) with a red light wavelength of 632.8 nm and a blue light wavelength of 405 nm. An emulsion sample was drop-wise added to circulating distilled water, which had been adjusted to the same pH as that of the emulsion. A volume and number weighted mean diameter and size distribution of particles were recorded after 20 scans.

### Rubber Compounding

Rubber compounding was conducted with a Brabender mixer (ATR Plasti-corder, C.W. Brabender Instruments, South Hackensack, NJ) equipped with a pair of Banbury blades. The mixing bowl has a sample volume of 52.5 mL after it was filled to 70% of the total volume (75 mL) for all sample preparations. The volume of all formulations (Table I) was fixed at 52.5 mL calculated from the components' densities. The dried natural rubber blends with soy protein prepared as described in the previous section was fed into a Brabender internal mixer along

**Table I.** Rubber Formulation[a]

| CB/SP ratio | | 1/3 | 1/1 | 3/1 |
|---|---|---|---|---|
| 10% filler | SP | 2.8 | 5.6 | 8.4 |
| | CB | 8.4 | 5.6 | 2.8 |
| 20% filler | SP | 6.25 | 12.5 | 18.75 |
| | CB | 18.75 | 12.5 | 6.25 |
| 30% filler | SP | 10.7 | 21.4 | 32.1 |
| | CB | 32.1 | 21.4 | 10.7 |
| 40% filler | SP | 16.65 | 33.3 | 49.95 |
| | CB | 49.95 | 33.3 | 16.65 |

[a] The amount of ingredients in the formulations is represented by phr (parts per hundred parts of rubber). Other components are the same in all formulations: natural rubber = 100, anti-oxidant = 0.8, stearic acid = 2, zinc oxide = 3, accelerator = 1, and sulfur = 2.

with carbon black (N339) and other ingredients (antioxidant, rubber, zinc oxide) at 80°C, and mixed at 60 rpm for 20 min, which included 5 min of feeding time. The mixture was then cooled to 100°C, followed by the addition of sulphur and accelerator, and mixed for 3 min. The natural rubber composites thus prepared contain a SP/CB ratio of 1/3, 1/1, and 3/1 (Table I). The composites with 10, 20, 30, and 40 wt % filler in terms of total weight of the filler and rubber were prepared (Table I). The final compounds were compression molded in a window-type mold at 4 MPa and 160°C for 15 min. The curing time used was beyond the fully cure stage for all the samples; it also provided the same thermal history for all the samples. After the compression molding, the samples were relaxed and annealed at 140°C for 1 h.

### Stress–Strain Measurements

The compounded rubber samples were moulded into ring test specimens (ASTM D638) with a ring shape mould, which has an inner and outer diameter of 26 and 30 mm, respectively. The ring sample has a thickness of 3 mm. Compared with a dog bone sample, a ring sample does not use grip and therefore does not have slippage effect associated with soft samples. Stress–strain measurements were conducted with an Instron 4201 tensile testing machine (Instron, Norwood, MA) equipped with a 1 KN load cell and operated at a crosshead speed of 8.3 mm/s.

### Dynamic Mechanical Measurements

Linear viscoelastic properties in shear mode were studied with a strain-controlled rheometer. A Rheometric ARES-LSM rheometer (TA Instruments, Piscataway, NJ) with TA Orchestrator software was used for the dynamic mechanical measurements. The instrumental method and the sample preparations are highly reproducible. To study thermal mechanical properties of the composites, temperature ramp experiments were conducted with torsion rectangular geometry at a heating rate of 1°C/min in a temperature range from −68 to 140°C. When torsion rectangular geometry was used, torsional bars with dimensions of approximately 50 × 12.5 × 6 $mm^3$ were mounted between a pair of torsion rectangular fixtures, and the dynamic mechanical measurements were conducted at a frequency of 0.16 Hz (1 rad/s) and a strain of 0.05%. Frequency sweep experiments were conducted in a frequency range of 0.1 to 100 rad/s and a temperature range of −65 to 75°C. The strain sweep experiments were conducted at 1 Hz and in a strain range of 0.02–20%. Eight consecutive cycles were conducted for each composite and only minor changes were observed after the fourth cycle, therefore the eighth cycle was taken as a reversible cycle.

## RESULTS AND DISCUSSION

### Stress–Strain Properties

Stress–strain curves of natural rubber and the composites with 10–40% total fillers are shown in Figure 2. The fillers include soy protein (SP) nano-aggregates, carbon black (CB) and CB/SP with a ratio of 3/1 are shown in Figure 2. The stress–strain behavior of the natural rubber exhibits its typical behavior with an upturn occurred at the higher elongation ratios, which is attributed to stress-induced crystallization.[19,20] The composite

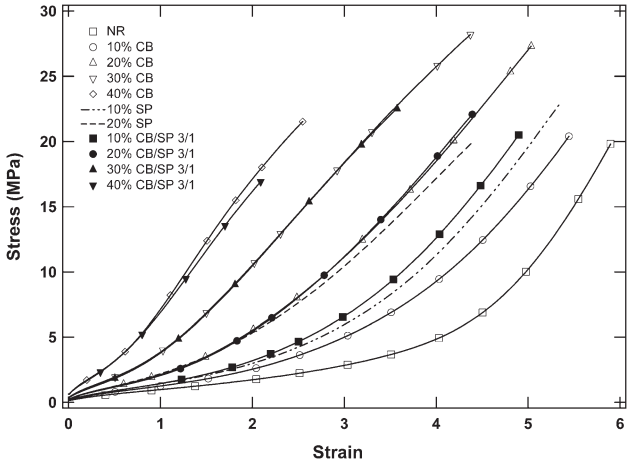


**Figure 2.** Stress–strain curves from the natural rubber and composites with 10–40 wt % total fillers.

with 10% protein filler shows a higher stress at the same elongation ratio compared with the composite with the 10% carbon black filler. The better stress–strain property of the 10% protein composite can be attributed partly to its greater filler volume fraction because soy protein has a smaller density (1.3 $gm/cm^3$) compared with carbon black (1.72 $gm/cm^3$). Other factors such as filler-polymer adhesion will be discussed later. The composite with 20% protein filler, however, starts to show a slightly less stress at the higher elongation ratios compared with the composite with 20% carbon black. We have tested the composites with three different CB/SP ratios (3/1, 1/1, and 1/3). The composites with 3/1 CB/SP ratio had a stress–strain behavior most resemble to that of the carbon black composites shown in Figure 2. The composite with 10% filler composed of 3/1 CB/SP even showed a synergistic effect with a higher tensile stress compared with both 10% protein and carbon black filled composites at the same elongation ratios. Although a 25% substitution of carbon black with protein decrease the tensile strength at break for the 3/1 CB/SP composites, they still retain useful breaking tensile strength at about 20 MPa. Because a large volume of carbon black from petroleum source is consumed annually, a potentially 20% replacement with a renewable content is significant for environmental and sustainability reasons.

### Analysis of Stress–Strain Behaviors with Micromechanical Model

Theoretical description of rubber elasticity has been evolving and continuously developed since early 1900.[21,22] For most practical applications, rubbers are reinforced with fillers. For these filled rubbers, the current understanding is that there are modulus contributions from polymer network, polymer-filler interactions, filler network, and hydrodynamic amplification.[23] The development based on the tube model to describe stress–strain isotherms have been shown to describe the experimental data reasonably well.[24,25] In this study, the model based on the generalized tube model and strain-induced breakdown of fractal filler and filler network[24] is used to analyze the experimental stress–strain curves. For uniaxial extension, the stress was described as[24]

$$\sigma = G_c\left(\lambda - \lambda^{-2}\right)\left\{\frac{1-T_e/n_e}{\left(1-\frac{T_e}{n_e}\left(\lambda^2+2/\lambda-3\right)\right)^2}-\frac{T_e/n_e}{1-\frac{T_e}{n_e}\left(\lambda^2+2/\lambda-3\right)}\right\}+2G_e\left(\lambda^{-1/2}-\lambda^{-2}\right) \quad (1)$$

where $\sigma$ is stress, $G_c$ is the elastic modulus from crosslinking constraints, $\lambda$ is strain, $T_e$ is a trapping factor between 0 and 1, $n_e$ is the mean number of statistical segments between two successive entanglements, $G_e$ is the elastic modulus from topological tube-like constraints. The intrinsic strain ratio $\lambda$ in eq. (1) is related to the external deformation $\varepsilon$ through a deformation dependent amplification factor $X(\varepsilon)$ as follows: [24]

$$\lambda = 1+X(\varepsilon)\varepsilon \approx 1+(X_\infty+(X_0-X_\infty)\exp(-z\varepsilon))\varepsilon \quad (2)$$

where $X_0$ and $X_\infty$ are respectively the amplification factor at zero and infinite strain limits, $z$ is an empirical parameter related to the strength and stiffness of the filler clusters and the elastic modulus of the polymer matrix. Although $X(\varepsilon)$ was also suggested to have a power law expression for some rubber composites,[24,25] it was found that the exponential decay law in eq. (2) gave a better description of the stress–strain curves in this study.

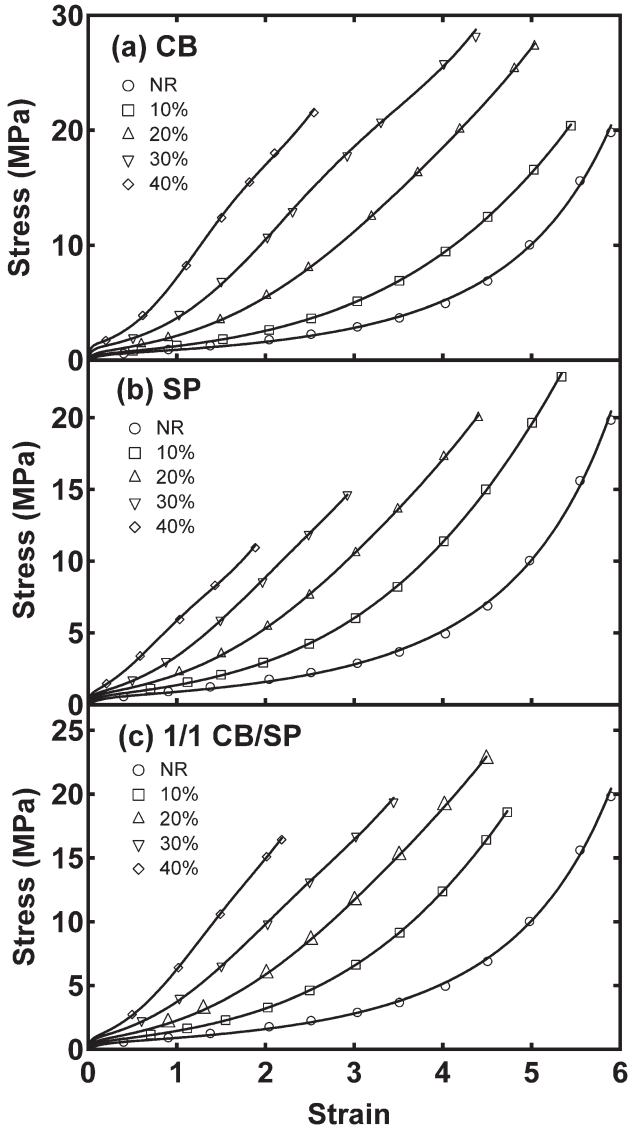


**Figure 3.** Stress–strain curves fitted with eq. (1).

The modeling of the stress–strain curves from CB, SP and 1/1 CB/SP composites are shown in Figure 3. The fitting of the model to the experimental data is very good for all three series of the samples. The amplification functions $X(\varepsilon)$ that yield a good fit to the experimental data in Figure 3 are shown in Figure 4. Comparing $X(\varepsilon)$ of the CB composites with that of SP composites in Figure 4(a), it shows that $X(\varepsilon)$ of SP composites decay faster and implies that the breakdown of protein filler network has a greater dependence on the strain. This filler network breakdown behavior explains why the 20% SP composites has a lower stress at the higher elongation ratio compared with the 20% CB composites in Figure 2. Figure 4(b) shows similar decay behavior for the 1/1 CB/SP composites with the decay becoming more significant as the total filler fraction increases. Another way to look at the higher strain behavior of these composites is to look at the reduced stress $[\sigma^*] = \sigma/(\lambda - \lambda^{-2})$ plotted against the reciprocal of the extension ratio. This representation came from the empirical Mooney–Rivlin equation[26]

$$\sigma^* = 2C_1 + 2C_2\lambda^{-1} \quad (3)$$

where $2C_1$ and $2C_2$ are constants independent of $\lambda$. The plot is sensitive in showing the upturns of stress–strain curves at higher elongation ratios. Figure 5 shows such plots for CB, SP, and 1/1CB/SP composites. The upturn for the unfilled NR is associated with stress-induced crystallization.[19,20] For unfilled rubbers that do not undergo stress-induced crystallization with increasing strain, the reduced stress usually decreased ascribed to the transition from affine network to phantom network.[21] The 40% CB composite has a significant upturn caused by limited chain extensibility compared with the 40% SP composite. The 40% 1/1 CB/SP composite shows an upturn behavior similar to that of the 40% CB composite. The reduced stress behavior of 40% SP composite indicates both a greater dependence of filler network breakdown with strain and less ability to induce crystallization at higher strains. A different behavior was observed for the 10% SP composite. Its upturn occurred at a smaller strain than the 10% CB composite, indicating a greater ability to induce crystallization at a lower strain. The 10% 1/1 CB/SP composite showed similar upturn behavior to the 10% SP composite.

The model fitting using eq. (1) also generates parameters, $G_c$, $G_e$, and $n_e/T_e$. These parameters are plotted against filler fraction for each series of composites in Figure 6. It was found that better fit can be obtained when $n_e/T_e$ value is fixed for all samples. This is reasonable because $n_e/T_e$ is proportional to crosslink density, which was formulated to be the same by using same

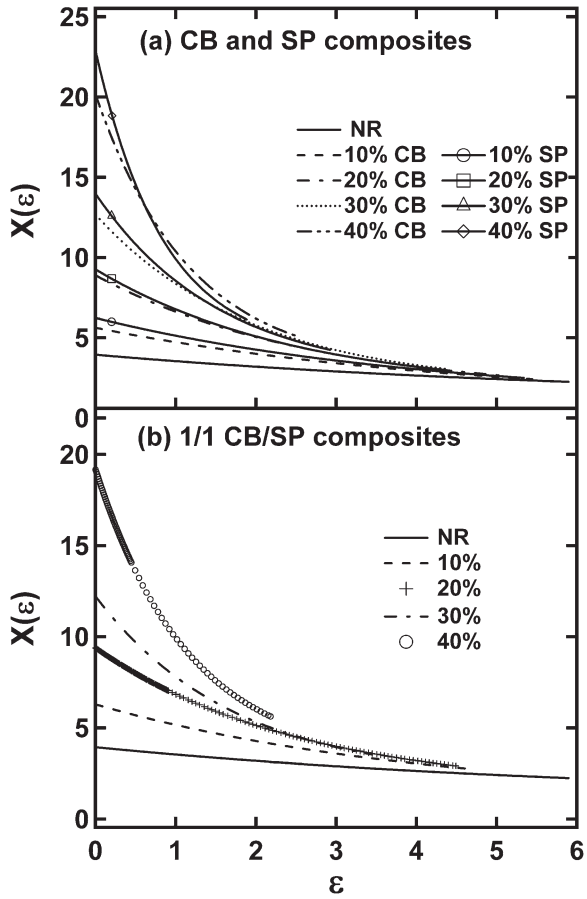


**Figure 4.** Strain amplification factors for the CB, SP, and 1/1 CB/SP composites.

amount of sulphur and accelerator as shown in Table I. In the current fitting procedure, $n_e/T_e$ was obtained by fitting stress–strain curve of unfilled natural rubber with $G_e \approx 0.29$ MPa, which is approximately one half of the plateau modulus $G_N^0$ of NR-melts.[27] The modulus $G_c$ is proportional to crosslink density. In Figure 6(a–c), $G_c$ increases slightly with the increasing filler fraction. This is to be expected because fillers also act as multifunctional physical crosslinks through the adsorption of

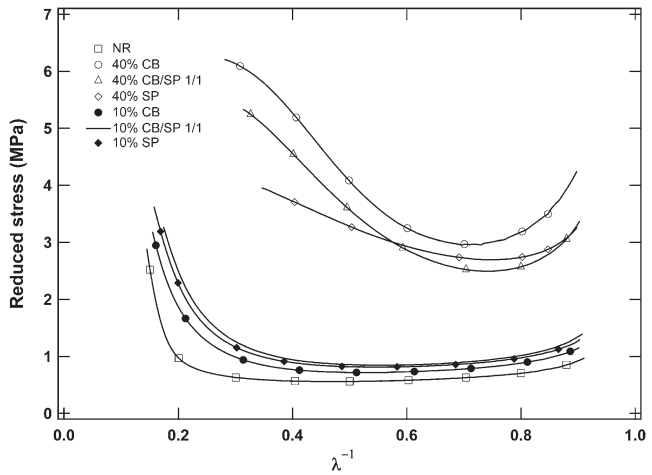


**Figure 5.** Reduced stress for CB, SP, and 1/1 CB/SP composites.

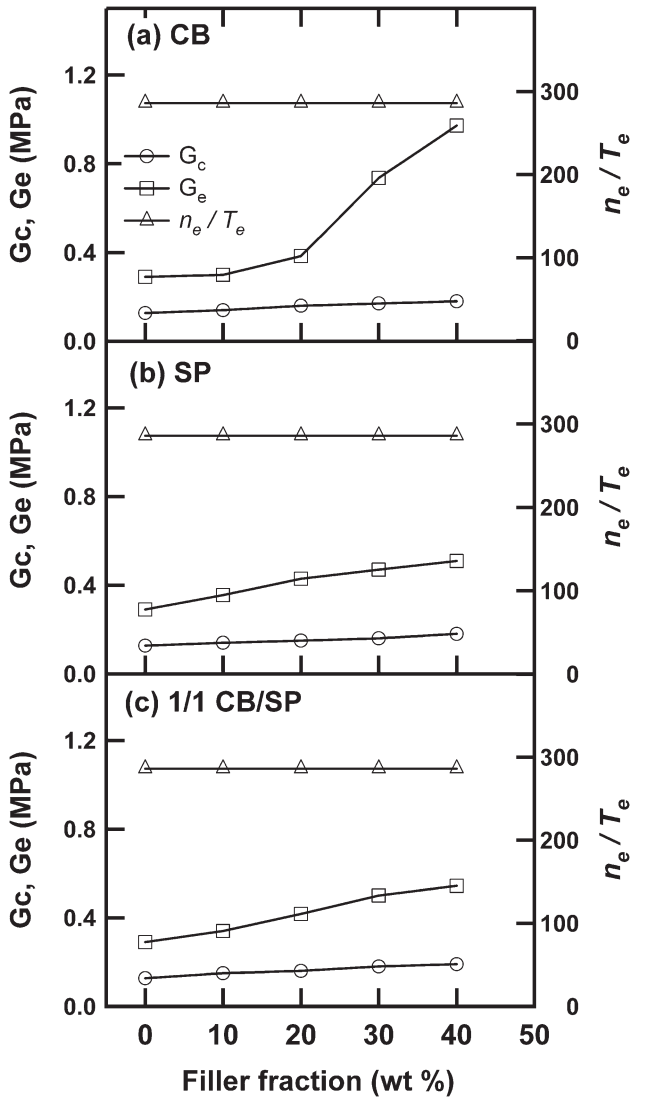


**Figure 6.** Fitting parameters, $G_c$, $G_e$, and $n_e/T_e$

polymer chains on the filler surface.[28] Although $T_e$ was said to increase with increasing crosslink density,[24] the $n_e/T_e$ values were found to be not sensitive to the additional physical crosslinks created by increasing filler fractions. The most significant difference observed in Figure 6 is the change of modulus $G_e$ with the increasing filler fraction. The CB composites show a significant increase in $G_e$ when the filler fraction increases from 20 to 30 and 40%. Because the modulus $G_e$ is proportional to the entanglement density of the rubber composites, the data indicates that carbon black generates more effective entanglements than the soy protein filler at higher filler fractions. However, another factor that can also increase the modulus is strain-induced crystallization of natural rubber[19,20] as mentioned above. The strain-induced crystallites can act as additional crosslinks and fillers,[29,30] and therefore also contribute to the moduli $G_c$ and $G_e$.

### Linear Viscoelastic Properties

Figure 7 shows the increase of elastic modulus with the increasing filler volume fraction for all composites as expected. The

Applied Polymer SCIENCE

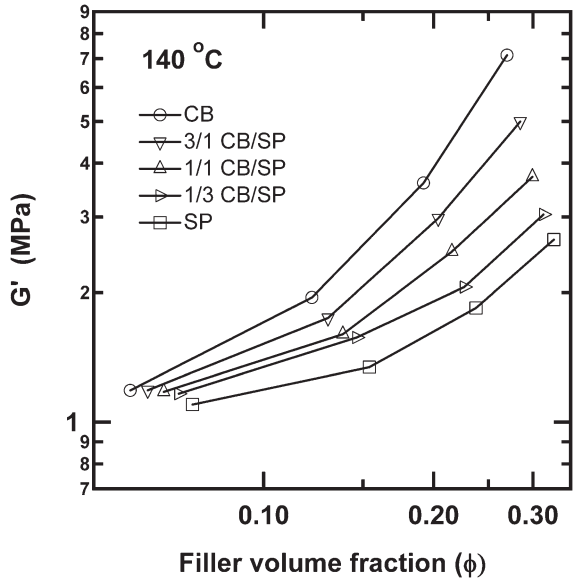


**Figure 7.** Elastic modulus of the composites at 140°C.

modulus also increases with the increasing volume fraction of the carbon black in the CB/SP composites, indicating carbon black forms a more rigid filler network than soy protein. The log–log plots showed a near straight line only above about 20 wt % filler fraction and is an indication that the gel point of the filler network for these composites is above about 20 wt % filler fraction because $G' \propto \varphi^k$ for fractal aggregates[23] above the mechanical gel point of a filler network. The modulus of the filler network for all composites is temperature dependent as shown in Figure 8. The reinforcement factor, $G'/G_0'$, in Figure 8 is significantly higher at 25°C than at 140°C. This indicates the softening of filler network caused by the increasing flexibility of polymer chains immobilized by the filler particles as the temperature increased. The immobilization of polymer chains has been estimated as a thin hard shell[31] around the filler particles and possibly also has a longer range effect.[32] The volume fraction dependence of reinforcement factor is described by Guth–Gold[33] equation for rubber composites with a soft filler network.

$$G' = G_0'\left(1+2.5\phi+14.1\phi^2\right) \quad (4)$$

where $G_0'$ is the modulus of the matrix and $\phi$ is the volume fraction of the filler. The equation is known to be unable to describe rubber composites with a more rigid filler network. Figure 8(a,b) show a smooth line calculated with the Guth–Gold equation. Only the protein composites at 140°C in Figure 8(a) have a reasonable fit with this equation. At 25°C, none of the composites in this study can be described by this equation. The effect of temperature to soften the filler network is known through the strain sweep experiments at different temperatures in both silica filled natural rubber[34] and styrene-butadiene rubber,[28] where the amplitude of Payne effect, $\Delta G' = G_0' - G_\infty'$, decreased with increasing temperature. This was interpreted as the softening of filler–filler and filler–polymer interactions.[35,36] Consistent with those previous studies, the soy protein composites were affected by temperature at 140°C and have a softer and more elastic filler network. The interactions between the protein particles and the polymer chains are reduced at the higher temperature and the filler network are softened enough by the high temperature to be described by the Guth–Gold equation. Smaller magnitude of polymer–filler interactions, in terms of number and strength, also means polymer chains are less confined by the filler surface, and therefore do not reach their limited extensibility at a higher strain compared with the polymer chains strongly adsorbed by the carbon black surface. The limited chain extensibility is a required condition for orientation-induced crystallization to occur. Therefore, smaller polymer–filler interaction in the protein composites means the extent of strain-induced crystallization for protein composites at a higher strain is reduced. Such mechanism can explain the less upturn behavior of the 40% protein composite compared with the 40% CB or 40% 1/1 CB/SP composites in Figure 5.

The immobilization effect of filler on polymer chains can also be understood from the variation of elastic modulus with frequency in Figure 9, where the time-temperature superposition was obtained from a good fit to WLF equation.[37] In the glass transition region, $G'$ is proportional to $\omega^1$ and the slope decreased to 3/5 for the composite with 40% protein filler. This is similar to theoretical estimate of filled rubber with $G' \propto \omega^{3/4}$ for the unfilled rubber and $G' \propto \omega^{3/8}$ for the highly filled rubber with 50 wt % filler.[23] The decrease in the slope is because of the greater restriction on the mobility of polymer chains by

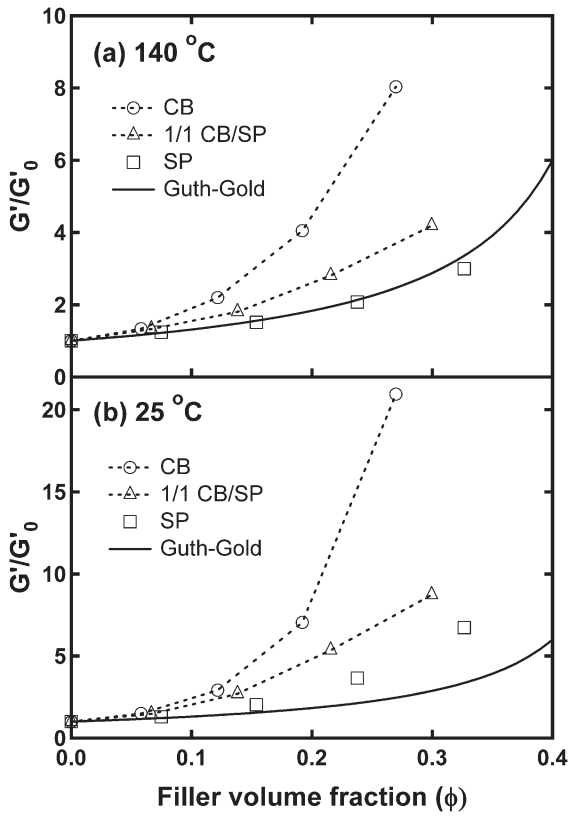


**Figure 8.** Reinforcement factor, $G'/G_0'$, for CB, SP, and 1/1 CB/SP composites. $G'$ is the elastic modulus of the composites and $G_0'$ is the elastic modulus of the natural rubber.

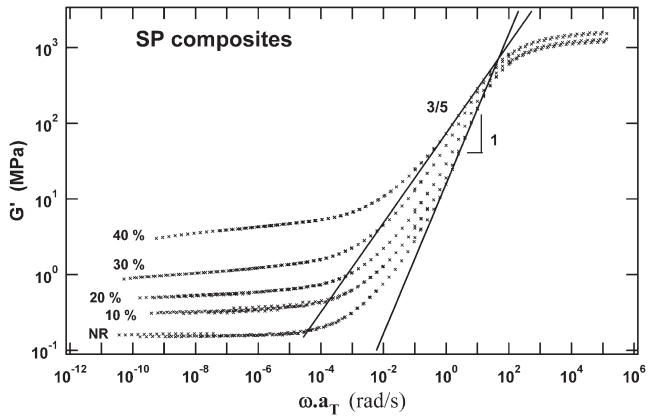


**Figure 9.** Elastic moduli of the natural rubber and the soy protein composites with 10–40 % filler are plotted against frequency reduced to −55°C.

the filler surface.[23,28] Compared with the 40% carbon black composite, which has a slope of $G' \propto \omega^{1/2}$, it can be deduced that $G' \propto \omega^{3/5}$for the 40% protein composite indicates that the protein surface has less constraint on the polymer chains.

### Nonlinear Small Strain Properties

Nonlinear properties of filled rubber composites are usually investigated with dynamic strain sweep experiments because of a greater dependence of elastic modulus on strain compared with unfilled rubbers. The effect is known as Payne effect and is interpreted as breakdown of a filler network.[35,36] The decrease of elastic modulus with increasing strain is dominated by the characteristics of filler network in highly filled rubber,[21] but also occurs in rubbers with filler concentrations below percolation threshold.[38] The strain range (ca., 20%) investigated in this study is corresponding to the strain range in the beginning of the stress–strain isotherms. Figure 10 shows the stress softening in natural rubber and 10% filled rubber composites. The curves in Figure 10 are the eighth strain cycle and therefore represent a reversible cycle. Figure 10(a) shows that the crosslinked natural rubber is inhomogeneous and consisted of regions with different modulus. Each segment of the broken curve in Figure 10(a) represents regions with a certain modulus. As this is a reversible curve (the eighth strain cycle), the broken segments of the curve signalled different stages of network unfolding, as opposed to network breakage in an irreversible cycle. Each stage of network unfolding appeared to resist the increasing stress and relaxed suddenly when the network structure of those regions represented by each curve segment unfolded. This interpretation is consistent with a neutron scattering study, which showed that natural rubber is inhomogeneous because of the presence of NR protein aggregates.[39] For the crosslinked natural rubber, it also contained zinc oxide and other solid ingredients that can act as fillers, therefore the filler effect of these additives cannot be excluded. For natural rubber without deproteinization, such as the natural rubber used in this study, the distance between protein aggregates was estimated to be about 25 nm by the neutron scattering.[39] With such a short distance, the addition of other additives will likely form zones of localized filler network structure with different modulus and may account for the observation in Figure 10. Localized filler network structure is best described by a cluster-growth mechanism,[40] where filler clusters form first before they grow larger and merge into each other to form an infinite filler network at the gel point of the filler network. The effect shown in Figure 10(a) for the unfilled natural rubber also persisted for all 10% filled composites, indicating the 10% filled composites are below the gel point of their filler networks. This observation is consistent with Figure 7, which indicates the gel point of the filler network is above 20 wt % filler. The effect observed in Figure 10 became insignificant for the 40% filled composites in Figure 11. The curves in Figure 11 are fitted with the Kraus model.[33]

$$\frac{G'(\gamma)-G'_\infty}{G'_0-G'_\infty}=\frac{1}{1+(\gamma/\gamma_c)^{2m}} \quad (5)$$

where $G'_\infty$ is equal to $G'(\gamma)$ at very large strain, $G'_0$ is equal to $G'(\gamma)$ at very small strain, $\gamma_c$ is a characteristic strain where

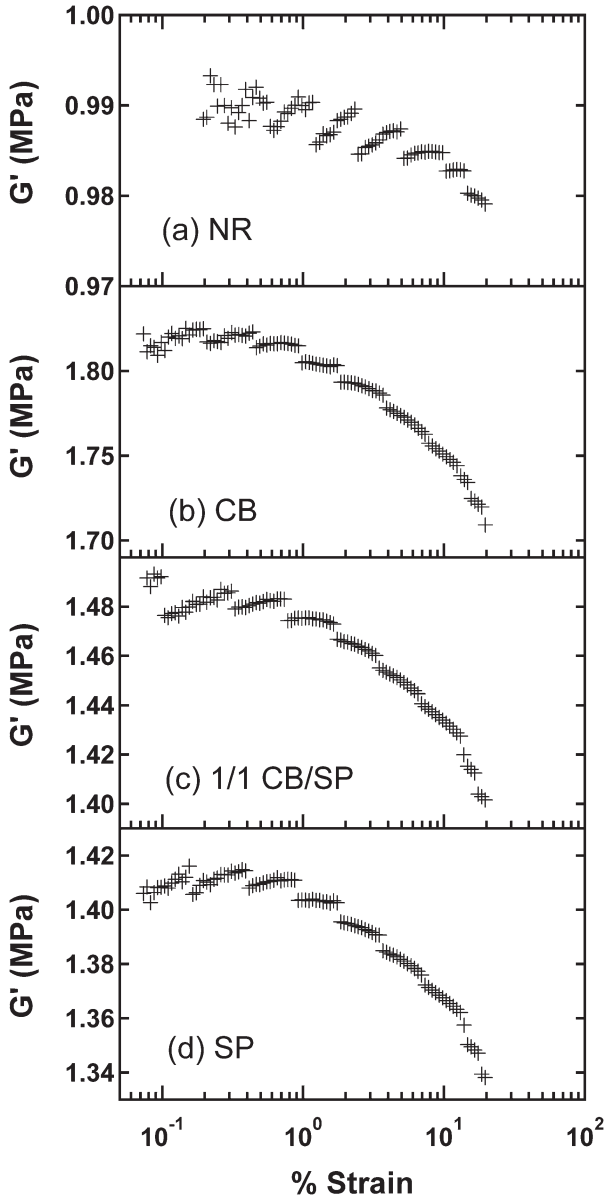


**Figure 10.** Variation of elastic modulus as a function of strain for the 10% composites.

$G_0' - G_\infty'$ is reduced to half of its zero-strain value, and $m$ is a fitting parameter related to filler aggregate structures.[23] Equation (5) has been shown to describe the behavior of $G'(\gamma)$ in carbon black filled rubber reasonably well.[21]

Figure 11 shows that the amplitude of the Payne effect decreased with increasing protein concentration. Previous observations showed that the amplitude of the Payne effect decreases with increasing temperature[28,36] and the effect was attributed to increasing mobility of polymer chains that connect fillers and/or the dissociation of filler–filler bonds. The smaller amplitude of the Payne effect for the 40% protein composite in Figure 11 may be interpreted as the filler network of soy protein is softer and elastic. The critical strains, $\gamma_c$, for the 40% composites are also shown in Figure 11 and it shows that $\gamma_c$ increases with increasing soy protein concentration. The elasticity of a filler network is considered to be determined by the flexibility of bridges between fillers. These bridges can be a polymer bridge or direct filler–filler bonds, or the combination of both. For a filler network that is dominated by polymer bridges, it has been observed that factors such as temperature [34,41] that can increase

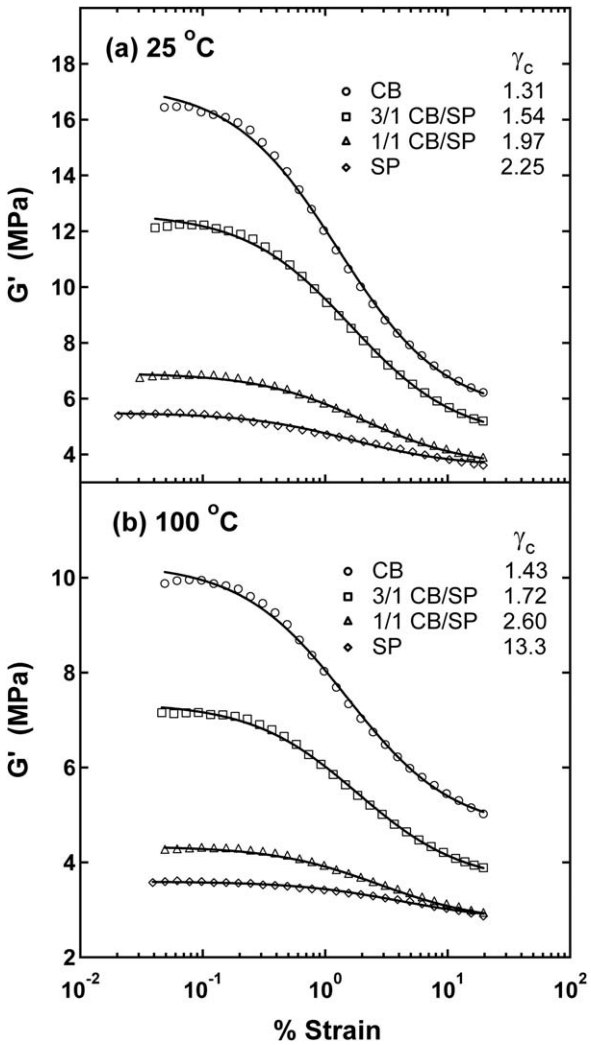


**Figure 11.** Variation of reversible elastic modulus as a function of strain for the 40% composites. The solid lines are the model fittings.

**Table II.** Stress Modulus at 100% Elongation

| | 10% composites (MPa) | 40% composites (MPa) |
|---|---|---|
| CB | 0.9 | 9.89 |
| 3/1 CB/SP | 1.19 | 8.93 |
| 1/1 CB/SP | 1.23 | 8.42 |
| 1/3 CB/SP | 1.26 | 7.12 |
| SP | 1.25 | 5.95 |

the mobility of polymer chains tend to increase the value of $\gamma_c$. Comparing $\gamma_c$ in Figure (a) and (b), it shows that the values of $\gamma_c$ shift to higher strains as the temperature increased from 25 to 100°C. The most significant change is the $\gamma_c$ for the 40% soy protein composite (Figure 11) and is an indication that its filler network is significantly softened by the higher temperature, consistent with the trend of reinforcement factors in Figure 8. For surface modifications[28] that disrupt filler–filler bonds with flexible polymer chains also caused $\gamma_c$ to shift to a higher strain. From these previous studies, it can be deduced that the composites with higher protein concentration have filler networks that were more soft and flexible, caused by lesser constraint on the polymer chains. The same interpretation was obtained by applying the Maier–Goritz model,[42] which emphasizes the polymer bridges between fillers, to fit the data in Figure 11. The result indicates that the $G'$ contributions from both stable and unstable polymer–filler interactions decreased with the increasing protein concentration, indicating soy protein has less constraint on the polymer chains similar to the trend observed in the case of increasing temperature.[34] However, a softer filler network for the soy protein composites with higher filler content does not explain good tensile properties observed in the 10% soy protein composite. For the composites below the gel point of filler network, filler–polymer adhesion plays an important role. For the 10% soy protein composite, its good tensile properties can be attributed to its good adhesion to natural rubber by using the NR protein as a compatibilizer. As the soy protein concentration increased, the filler–polymer adhesion decreased because of the limited amount of NR protein available in the natural rubber. The NR protein content in natural rubber varies from 1 to 1.8% depending on genetic, chemical, and metabolic makeup of the rubber tree.[43,44] The studies on the silica filled styrene-butadiene rubber composites have shown that the work of adhesion between filler and polymer is proportional to stress modulus at 100% elongation.[28] Table II shows the stress modulus at 100% elongation for the 10 and 40% composites. The trend confirms that filler–polymer adhesion is greater for the 10% composites with higher soy protein concentration, while the trend is reversed for the 40% composites.

## CONCLUSIONS

The stress–strain properties of the composites investigated in this study show that natural rubber composites filled with 10% soy protein nano-aggreagtes has excellent tensile properties and has a synergistic effect when melt-processed with carbon black

at 25% substitution level. Rubber composites with 25% substitution of carbon black with soy protein showed competitive tensile properties for the 10–40% filled composites. The stress–strain isotherms were analyzed using a micromechanical model based on the generalized tube model and the model fittings showed that the strain amplification factor of the soy protein composites were more sensitive to the increasing strains, indicating the filler network of the soy protein composites dissociated more rapidly with increasing strain compared with the carbon black composites. The entanglement modulus, $G_e$, from the model fitting also indicates the soy protein composites had less constraint on the polymer chains to create more entanglements. The reinforcement factors show that the soy protein composites softened more by the increased temperature and had a filler network soft enough to be described by the Guth–Gold equation. The variation of elastic modulus with oscillatory frequency shows that $G' \propto \omega^{3/5}$for the 40% protein composite has a frequency-dependent slope greater than that of the 40% carbon black composite,$G' \propto \omega^{1/2}$, and is an indication that the protein surface has less constraint on the polymer chains. The nonlinear viscoelastic properties investigated with strain sweep experiments show that the 10% composites had an inhomogeneous localized filler network structure represented by the segmented curves of reducing elastic modulus with increasing oscillatory strain. For the highly filled 40% composites, the critical strain, $\gamma_c$, increased with the increased temperature and was increased most significantly for the 40% filled soy protein composite, signalled the polymer chains were less constrained by the soy protein surface. For the composite reinforced with 10% soy protein, 100% stress modulus increased with increasing soy protein concentration and the trend was reversed for the 40% filled composites. This can be attributed to the good adhesion between soy protein and natural rubber through the compatibilizing effect of the NR protein. The filler–polymer adhesion decreased as the soy protein concentration increased because of the limited amount of NR protein available in the natural rubber.

## ACKNOWLEDGMENTS

The author likes to thank Mr. Gary Grose for conducting Instron measurements on these composites.

## REFERENCES

1. Roberts, A. D. Natural Rubber Science and Technology; Oxford Unversity Press: London, **1963**.
2. Archer, B. L.; Barnard, D.; Cockbain, E. G.; Dickenson, P. B.; McMullen, A. I. In The Chemistry and Physics of Rubber-like Substances; Bateman, L. Ed.; MacLaren & Sons: London, **1963**.
3. Greve, H.-H. In Ullmann's Encyclopaedia of Industrial Chemistry; Wiley-VCH: Weinheim, **2000**.
4. Lu, F. J.; Hsu, S. L. *Rubber Chem. Technol.* **1987**, *60*, 647.
5. Gregg, C. E.; Macey, J. H. *Rubber Chem. Technol.* **1973**, *46*, 47.
6. Tanaka, Y. *Rubber Chem. Technol.* **2001**, *74*, 355–375.
7. Favier, F.; Chanzy, H.; Cavaille, *J. Macromolecules* **1995**, *28*, 6365.
8. Cao, X.; Dong, H.; Li, C. M. *Bimacromolecules* **2007**, *8*, 899.
9. Qi, Q.; Wu, Y.; Tian, M.; Liang, G.; Zhang, L.; Ma, *J. Polymer* **2006**, *47*, 3896.
10. Angellier, H.; Molina-Boisseau, S.; Lebrun, L.; Dufresne, A. *Macromolecules* **2005**, *38*, 3783.
11. Zhang, A.; Wang, L.; Lin, Y.; Mi, X. *J. Appl. Polym. Sci.* **2006**, *101*, 1763.
12. Wang M. *J. Rubber Chem. Technol.* **1998**, *71*, 520.
13. Leblanc, J. L. *Prog. Polym. Sci.* **2002**, *27*, 627.
14. Badley, R. A.; Atkinson, D.; Hauser, H.; Oldani, D.; Green, J. P.; Stubbs, J. M. *Biochim. Biophys. Acta* **1975**, *412*, 214.
15. Qi, G.; Venkateshan, K.; Mo, X.; Zhang, L.; Sun, X. *J. Agri. Food Chem.* **2011**, *59*, 9958.
16. Jong, L. *J. Appl. Polym. Sci.* **2005**, *98*, 353.
17. Jong, L. *Polym. Int.* **2005**, *54*, 1572.
18. Lyon, F.; Burgess, K. In Encyclopaedia of Polymer Science and Engineering, 2nd edn.; Kroschwitz, J. I. Ed.; Wiley: New York. **1985**.
19. Trabelsi, P. A.; Albouy, P.-A.; Rault, *J. Macromolecules* **2003**, *36*, 9093.
20. Trabelsi, P. A.; Albouy, P.-A.; Rault, *J. Macromolecules* **2002**, *35*, 10054.
21. Mark, J. E.; Erman, B. Rubber Elasticity. A Molecular Primer; Wiley-Interscience: New York, **1988**.
22. Bateman, L. The Chemistry and Physics of Rubber-like Substances; MacLaren & Sons: London, **1963**.
23. Vilgis, T. A.; Heinrich, G.; Kluppel, M. Reinforcement of Polymer Nano-composites—Theory, Experiments and Applications; Cambridge University Press: Cambridge, **2009**.
24. Kluppel, M.; Schramm, *J. Macromol. Theory Simul.* **2000**, *9*, 742.
25. Heinrich, G.; Kluppel, M.; Vilgis, T. A. *Curr. Opin. Solid State Mater. Sci.* **2002**, *6*, 195.
26. Van der Hoff, B. M. E.; Bickler, E. J. *J. Macromol. Sci. Chem. A1* **1967**, *1*, 747.
27. Fetters, L. J.; Lohse, D. J.; Richter, D.; Witten, T. A.; Zirkel, A. *Macromolecules* **1994**, *27*, 4639.
28. Stockelhuber, K. W.; Svistkov, A. S.; Pelevin, A. G.; Heinrich, G. *Macromolecules* **2011**, *44*, 4366.
29. Trabelsi, P. A.; Albouy, P. –A.; Rault, *J. Macromolecules* **2003**, *36*, 7624.
30. Litvino, V. M.; Steeman, P. A. M. *Macromolecules* **1999**, *32*, 8476.
31. Vieweg, S.; Unger, R.; Hempel, E.; Donth, E. *J. Non-Cryst. Solids* **1998**, 235–237, 470.
32. Jouault, N.; Vallat, P.; Dalmas, F.; Said, S.; Jestin, J.; Boue, F. *Macromolecules* **2009**, *42*, 2031.
33. Guth, E.; Gold, O. *Phys. Rev.* **1938**, *53*, 322.
34. Meera, A. P.; Said, S.; Grohens, Y.; Thomas, S. *J. Phys. Chem. C* **2009**, *113*, 17997.

35. Kraus G. *J. Appl. Polym. Sci. Appl. Polym. Symp.* **1984**, *39*, 75.

36. Merabia, S.; Sotta, P.; Long, D. R. *Macromolecules* **2008**, *41*, 8252.

37. Williams, M. L.; Landel, R. F.; Ferry, J. D. *J. Am. Chem. Soc.* **1955**, *77*, 3701.

38. Sun, J.; Song, Y.; Zheng, Q.; Tan, H.; Yu, J.; Li, H. *J. Polym. Sci. Part B: Polym. Phys.* **2007**, *45*, 2594.

39. Takeshi, K.; Ikeda, Y.; Yasuda, Y.; Kohjiya, S.; Shibayama, M. *Bimacromolecules* **2007**, *8*, 693.

40. Kluppel, M.; Heinrich, G. *Rubber Chem. Techol.* **1995**, *68*, 623.

41. Gauthier, C.; Reynaud, E.; Vassoille, R.; Ladouce-Stelandre, L. *Polymer* **2004**, *45*, 2761.

42. Maier, P. G.; Goritz, D. *Kautsch. Gummi Kunstst.* **1996**, *49*, 18.

43. Posch, A.; Chen, Z.; Wheeler, C. *J. Allergy Clin. Immunol.* **1997**, *99*, 385.

44. Kurup, V. P.; Alenius, H.; Kelly, K. *J. Int. Arch. Allergy Immunol.* **1996**, *109*, 58.